



Study on creep characteristics of mudstone with different initial water contents in soaking conditions and its engineering applications

Yingchao Gao¹ · Wei Wei¹ · Dongjie Hua¹ · Qinghui Jiang¹

Received: 22 November 2021 / Accepted: 9 August 2022 / Published online: 24 August 2022
© Springer-Verlag GmbH Germany, part of Springer Nature 2022

Abstract

Understanding the effect of impoundment on the creep characteristics of rock mass of reservoir slope is vital to prevent and mitigate reservoir-impoundment-induced landslide hazard. In the present work, the degradation of creep characteristics of mudstones with different initial water contents under different soaking conditions is studied. The results show that in unsoaking conditions the axial instantaneous strain and axial creep strain of mudstone increase with increasing initial water content, while the long-term strength decreases. The soaking condition has a great influence on the creep strain and long-term strength of unsaturated samples but little influence on saturated samples. Moreover, the impacts of water on creep characteristics are mainly related to the water content of the samples during testing. Based on the test results, a creep constitutive model considering water is established and verified to be reasonable. Finally, the proposed model is implemented to simulate the time-dependent deformation of the Majiagou landslide in the Three Gorges Reservoir after impoundment.

Keywords Mudstone · Soaking conditions · Initial water content · Creep · Effects of water · Creep constitutive model

Introduction

Impoundment of reservoirs is the main triggering factor for many landslides in reservoir areas (Yang et al. 2013; Wang et al. 2007; Hu et al. 2012). The 1963 Vajont landslide is one of the most impressive disasters in recent history. After 3 years of impoundment, approximately 300 million m³ of rock mass slipped into the newly created Vajont Reservoir, destroying villages and leading to more than 2000 casualties (Pablo and Hatzor 2018). In the Three Gorges Reservoir area of China, more than 5000 landslides have been identified since impoundment (Huang et al. 2020). For example, the Majiagou landslide, triggered after the first impoundment of the reservoir (Zhang et al. 2018), has been deforming with an average velocity of 130 mm/year since 2008 (He et al. 2018). To prevent and mitigate reservoir-impoundment-induced landslide hazard, it is necessary to study the effect of impoundment on the long-term deformation of rock mass of reservoir slope.

Extensive studies have been conducted during the past few years, to investigate the long-term deformation behavior of rock, including granite (Kumagai et al. 1986; Hashiba and Fukui 2016), tuff (Yang and Daemen 1997), shale (Herrmann et al. 2019), sandstone (Zhao et al. 2011), and many other rock types (Ston and Scrivener 2019; Brijes and Priyesh 2015; Yang et al. 1999; Doi et al. 2014). Dried samples are used in most of the above literature. In fact, water has a negative influence on the long-term strength and deformation properties of limestone (Liu et al. 2015). From the perspective of theoretical grounds, even small amounts of water can influence the creep behavior of rock salt (Urai et al. 1986). By comparing with the creep experiments of dry rock, Liu et al. (2013) found that the presence of water resulted in a quality deterioration of amphibolite with time prolong. The analysis of powerhouse cavern long-term stability under saturated conditions showed that the increasing pore water pressure tends to local failure of powerhouse cavern (Ghorbani and Sharifzadeh 2009). Therefore, the effect of water on rock properties cannot be neglected. Engineering rock mass may contain different water contents (Jia et al. 2009; Jiang et al. 2011). To study the effects of water content on the mechanical behavior of greenschist with different volumetric contents of chlorite, biaxial compression creep tests were carried out (Xiong et al. 2014). Lu and Wang (2017) conducted a series of multistage creep tests

✉ Qinghui Jiang
jqh1972@whu.edu.cn

¹ School of Civil Engineering, Wuhan University,
Wuhan 430072, People's Republic of China

performed on coal with different water contents to determine the relationship between water content and creep deformation.

The previous studies have considered the effect of water content on the creep behavior of rocks. In fact, the slope near reservoirs may be immersed for a long time after impounding of the dam. Under soaking conditions, the water-induced weakening effect is obvious (Tang et al. 2018). However, few studies on the creep deformation behavior of rock masses under immersion were reported. In an effort to characterize the effects of changes in water conditions on the strength and creep lifetime of rocks, Hashiba et al. (2018) conducted uniaxial compression creep tests of Sanjome andesite. Compared with specimens without immersion in water, Yu et al. (2019) found that the soaking specimens exhibited significant increases in both creep strain and creep strain rate. Compression creep tests of limestone under different hydraulic confining pressures were carried out by a self-developed testing system, which revealed that both the strain and creep strain rate increased with increasing hydraulic confining pressure (Liu et al. 2015). However, there are relatively few achievements on the creep behavior of soft rock containing different water contents under immersion. The creep constitutive model considering the effects of water on soft rock needs to be further studied.

In the present study, multistage creep tests of mudstones with different initial water contents under soaking conditions are conducted. At the same time, tests in un-soaking conditions are considered as the control group to understand the influences of immersion and water content on creep behavior. Based on the experimental results, a creep constitutive model considering water is proposed. This model is verified and applied to practical slope engineering.

Experimental method

Sample preparation

Silty mudstone is taken to study the effect of water on rock creep characteristics. Figure 1 presents the X-ray powder diffraction patterns of the silty mudstone. The silty mudstone used in this experiment is composed of quartz (47%), illite (46%) and albite (7%).

The specimens are cylindrical, 50 mm in diameter and 100 mm in height, as shown in Fig. 2. To reduce the dispersion of the test results, the densities and longitudinal wave velocities of samples are measured after eliminating the samples with obvious defects. Samples with similar densities and wave velocities are selected for the next tests.

Test equipment

Uniaxial compression tests and creep tests are carried out with a rock mechanical testing system. As shown in Fig. 3, the testing machine is improved to ensure the creep test can conduct under immersion. A water immersion device made of polymethyl methacrylate (PMMA) is placed on the bearing plate.

Test procedure

First, a water absorption test of mudstone is carried out. The samples are dried in an oven at 105 °C for 24 h. Then, in accordance with the methods for determining the water absorbability of rock, a water absorption curve is obtained (Zhou et al. 2016). Four samples are taken for the water absorption test to reduce the dispersion of the test results.

Fig. 1 X-ray powder diffraction patterns of the tested mudstone

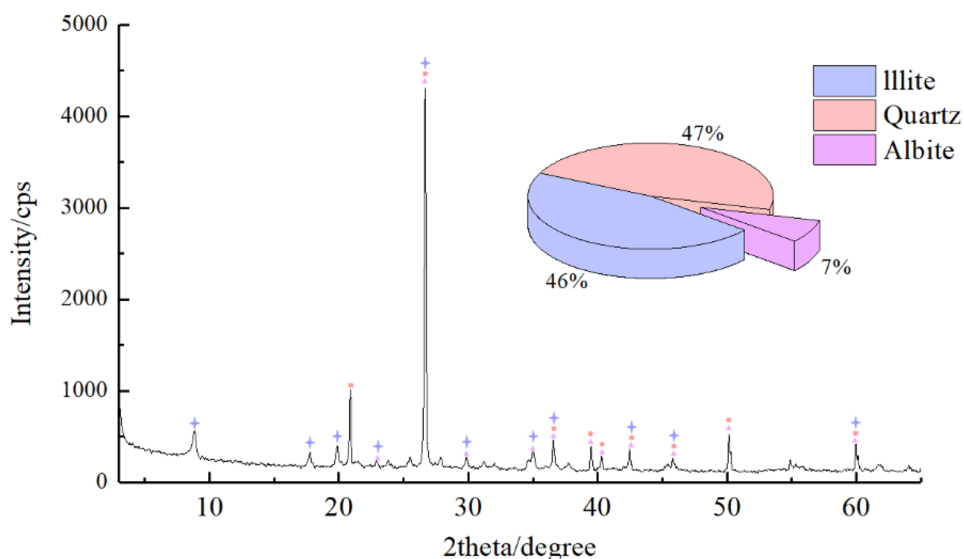


Fig. 2 Typical tested mudstone samples



The samples with different water contents are grouped into three sets. The first set of samples was dried at 105 °C for 24 h and denoted as the dried sample. The second set of samples was immersed for a specific time and denoted as the presoaked sample. The third set of samples was saturated in a vacuum ambient and denoted as the saturated samples.

Second, uniaxial compression creep tests on dried samples, presoaked samples and saturated samples are carried out under un-soaking and soaking conditions, respectively. To reduce the discreteness of the experimental data, more than two samples are subjected to each of the above treatments. To reduce the error caused by air humidity, the sample is sealed with wax under un-soaking conditions.

Axial stress is applied using 3 to 7 steps. Based on the compressive strength σ_0 , the axial stress of each step is determined into seven levels ($1/7\sigma_0$, $2/7\sigma_0$, $3/7\sigma_0$, $4/7\sigma_0$, $5/7\sigma_0$, $6/7\sigma_0$ and σ_0). The stress is applied step by step until the destruction of the specimen. The next loading step can be applied, while

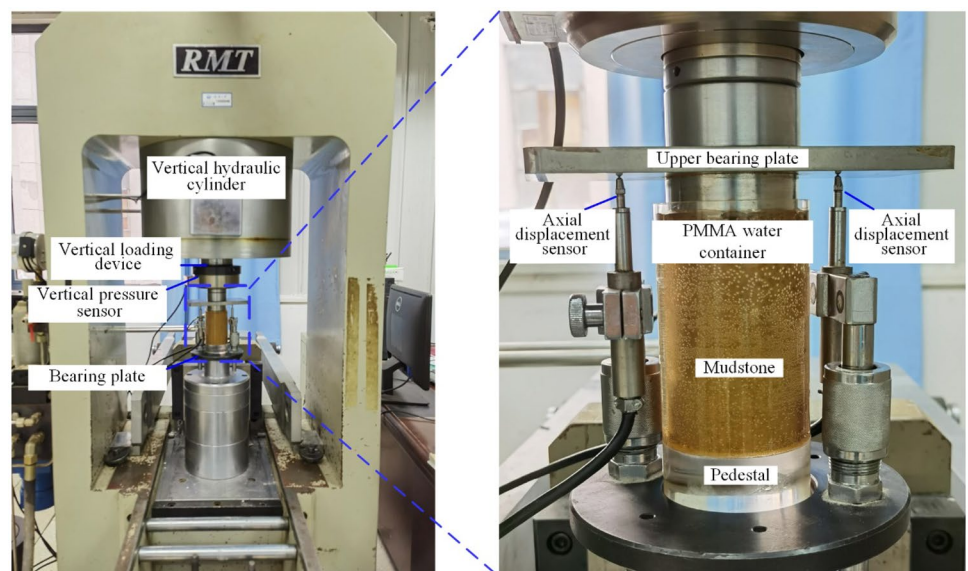
the sample is in a stable creep stage until the failure emerged. In the present work, all samples entered a steady-state creep stage within 24 h. Similar to relevant literature (Lu and Wang 2017; Yang et al. 2019; Wang et al. 2019b; Deng et al. 2016), each stress level is maintained for 24 h.

Experimental results

Water absorption test

Figure 4 shows the relationship between the average water content and soaking time of mudstone. Figure 4a shows that the water content of the samples increases rapidly from 0 to 16.4% in the first hour of soaking. From Fig. 4b, it takes approximately 2 days for the water content of the sample to increase from 16.4% to 18.4%, which indicates that the water absorption rate decreases slowly after soaking for 1

Fig. 3 The device for the multistage creep test under immersion



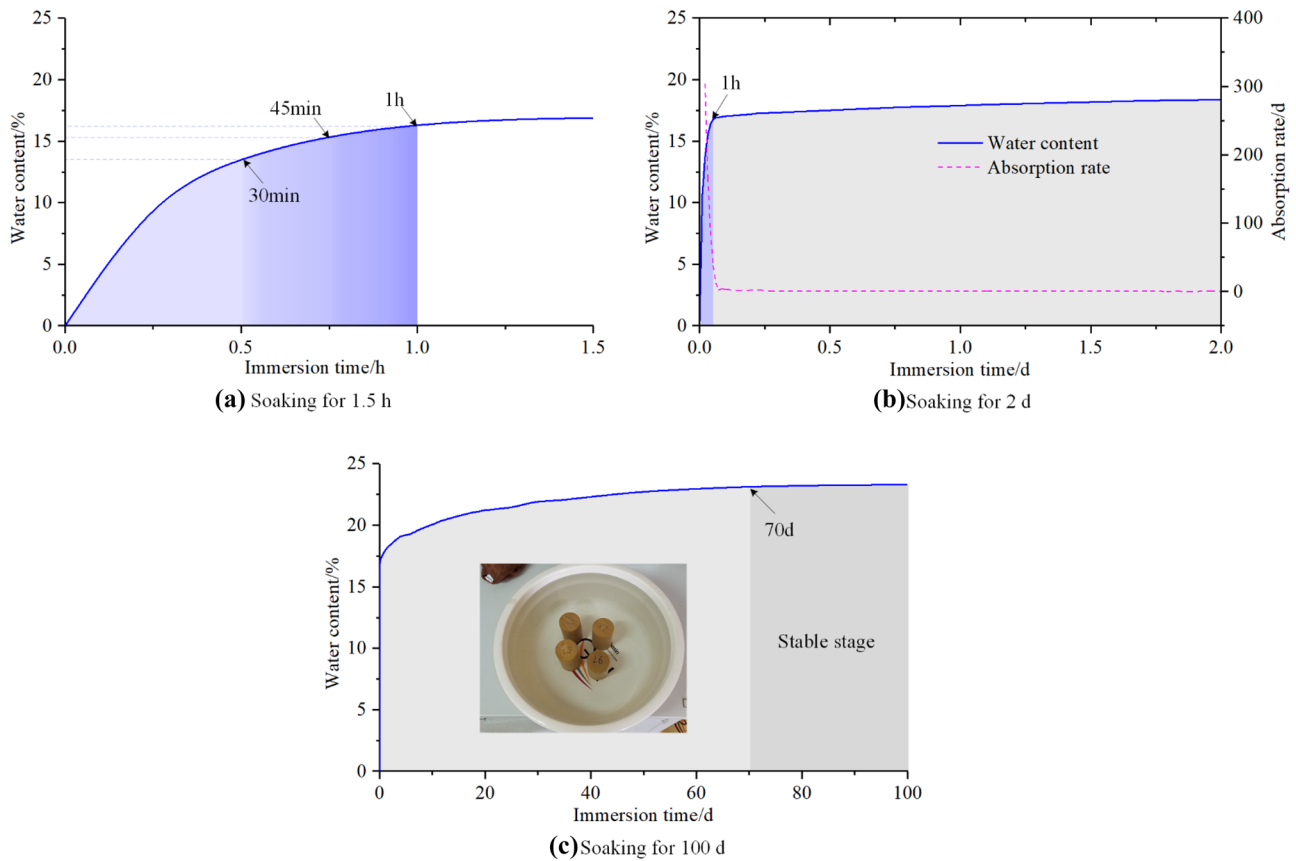


Fig. 4 Water absorption curve of mudstone

h. Hence, in the creep test, the water content is assumed to be stable within 1 h to 2 days after soaking. In practice, the water content of mudstone is completely stable after 70 days of immersion, and the saturated water content is 23.0%, as shown in Fig. 4c.

The water contents of the dried sample, presoaked sample and saturated sample were 0, 15.3% and 23.0%, respectively. The water content of the presoaked samples is determined based on the relationship between the soaking time, water content and water absorption rate. As seen in Fig. 4a, within 30 min of immersion, it is difficult to keep the water content at a specific value due to the high water absorption rate. The water content after soaking for 1 h was too large. For the reasons discussed above, the sample soaked for 45 min, with a water content of 15.3%, was taken as the presoaked sample.

Multistage creep test in the un-soaking condition

The uniaxial compression test shows that the average uniaxial compressive strength of dry mudstone samples in the un-soaking condition is 6.62 MPa. As mentioned previously, various axial stresses (0.95, 1.89, 2.84, 3.78, 4.73, 5.67 and 6.62 MPa) are applied step by step. Under un-soaking

conditions, the creep curves of the three sets of samples are shown in Fig. 5, where the ordinate ε is the axial strain.

Figure 5 shows that the failure strengths of the dried sample, presoaked sample and saturated sample are 6.62, 3.78 and 2.84 MPa, respectively. The time-to-failure is 7, 4 and 3 days, respectively.

In addition, the strains under each level of stress in the un-soaking condition are listed in Table 1. At a stress level of 0.95 MPa, the axial strains of the dried sample, presoaked sample and saturated sample are 0.81, 1.05 and 1.51, respectively. It can be concluded that with increasing water content, the strength of the sample decreases and the strain increases. The same conclusion can be drawn as the stress increases to 1.89 MPa.

Figure 6a illustrates the relationship between the strains (ε_0 , ε_c) and the stress level of samples in the un-soaking condition. An increase in the stress level leads to a decrease in the instantaneous strain ε_0 and an increase in the creep strain ε_c . The results also suggest that the strains (ε_0 , ε_c) increase with increasing water content: the strain of saturated samples is larger than that of both the presoaked and dried samples at the first two stress levels, and the strain of the presoaked samples is larger than that of the dried samples at the first three stress levels.

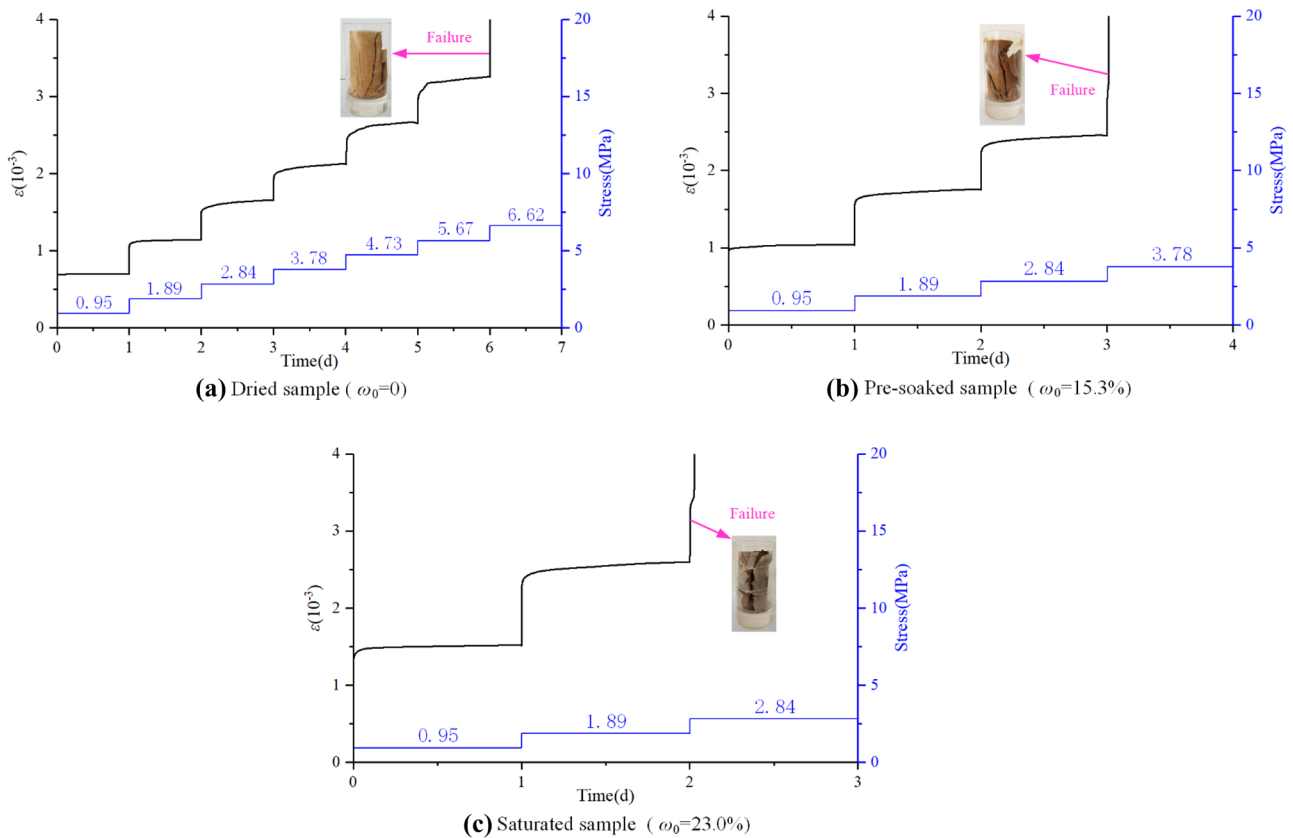


Fig. 5 Creep curves of samples in the un-soaking condition

The value of ϵ_c/ϵ , that is, the proportion of creep strain in the total strain, changes with stress and water content, as shown in Fig. 6b. First, the effect of stress on the value of ϵ_c/ϵ is discussed. For the dried samples, the creep strain is 0.12 at the first stress level (0.95 MPa), which accounts for 17% of the total strain. When the stress level increases to 5.67 MPa, the value of ϵ_c/ϵ increases to 60%. The result indicates that the value of ϵ_c/ϵ increases with increasing stress.

Then, the effect of the water content on the value of ϵ_c/ϵ is discussed. For instance, when the stress level $\sigma = 1.89$ MPa, the ϵ_c/ϵ values of the dried sample, presoaked sample and saturated sample are 23%, 30% and 36%, respectively. In general, the increase in the mudstone water content leads to the degradation of creep characteristics in un-soaking conditions.

Multistage creep test in the soaking condition

Figure 7 presents the creep curves of the dried sample, presoaked sample and saturated sample under soaking conditions. Additionally, the strains are listed in Table 2. Under the first stress level (0.95 MPa), the strain of the dried specimen decreased significantly soon after the instantaneous

deformation, and the deformation remained stable after 15 h. During the initial stage of immersion, there was a high rate of water absorption of the dried sample due to the existence of illite (see Fig. 4). As a result, the mudstone swelled, and the axial strain decreased significantly.

Under soaking conditions, the three sets of samples are all damaged at the third stress level (2.84 MPa). The failure modes of the three sets of samples are different. At the third stress level, the failure curve of the dried sample can be divided into three phases: deceleration, stable and accelerated creep phases. Brittle failure occurs in the presoaked and saturated samples; that is, failure occurs immediately after loading. However, the axial strain of the saturated sample is larger than that of the presoaked sample. Under soaking conditions, the larger the water content of the sample is, the more likely it is to be damaged.

Factors influencing creep characteristics due to water

Soaking conditions

The creep behavior of mudstone is different under un-soaking and soaking conditions. In terms of strength, the

Table 1 Strains of samples in the un-soaking condition

Sample	$\sigma = 0.95$ MPa			$\sigma = 1.89$ MPa			$\sigma = 2.84$ MPa			$\sigma = 3.78$ MPa			$\sigma = 4.73$ MPa			$\sigma = 5.67$ MPa								
	ϵ	ϵ_0	ϵ_c	ϵ_c/ϵ	ϵ	ϵ_0	ϵ_c	ϵ_c/ϵ	ϵ	ϵ_0	ϵ_c	ϵ_c/ϵ	ϵ	ϵ_0	ϵ_c	ϵ_c/ϵ	ϵ	ϵ_0	ϵ_c	ϵ_c/ϵ				
Dried	0.81	0.69	0.12	15%	0.45	0.35	0.10	23%	0.51	0.32	0.19	37%	0.47	0.25	0.22	47%	0.53	0.25	0.28	54%	0.60	0.24	0.36	60%
Presoaked	1.05	0.90	0.15	15%	0.70	0.49	0.21	30%	0.70	0.42	0.28	40%	-	-	-	-	-	-	-	-	-	-	-	
Saturated	1.51	1.25	0.26	17%	1.08	0.69	0.39	36%	-	0.57	-	-	-	-	-	-	-	-	-	-	-	-	-	

ϵ , ϵ_0 and ϵ_c are the total strain, instantaneous strain and creep strain, respectively. ϵ_c/ϵ is the proportion of creep strain in the total strain

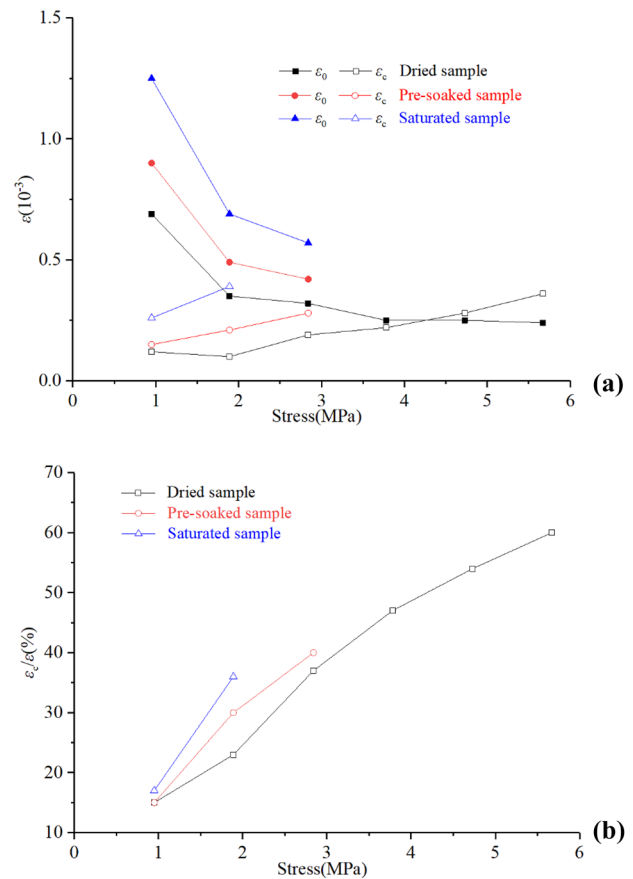


Fig. 6 Relationship between stress and **a** instantaneous strain ϵ_0 and creep strain ϵ_c and **b** the proportion of creep strain in total strain ϵ_c/ϵ

failure strengths of dried, presoaked and saturated samples under un-soaking conditions are 6.62, 3.78 and 2.84 MPa, respectively. Under soaking conditions, the failure strength of the three sets of samples is 2.84 MPa. Consequently, the strength of dried and presoaked samples under soaking conditions is significantly lower than that under un-soaking conditions.

In terms of creep strain, the variable α is defined (Yu et al. 2019), which is the ratio of the strain in the un-soaking condition to the strain in the soaking condition.

$$\alpha = \epsilon_{un-soaking} / \epsilon_{soaking} \times 100\% \tag{1}$$

Table 3 shows the α of the three sets of samples. The α of dried samples at $\sigma = 0.95$ MPa is neglected because the strain here includes the expansion deformation caused by water absorption.

It can be seen from Table 3 that, for the dried and presoaked samples, none of the values of α are less than 1, which suggests that compared with the un-soaking condition, the deformation under the soaking condition is larger. The α values of the saturated sample are 0.91 and 1.03. This

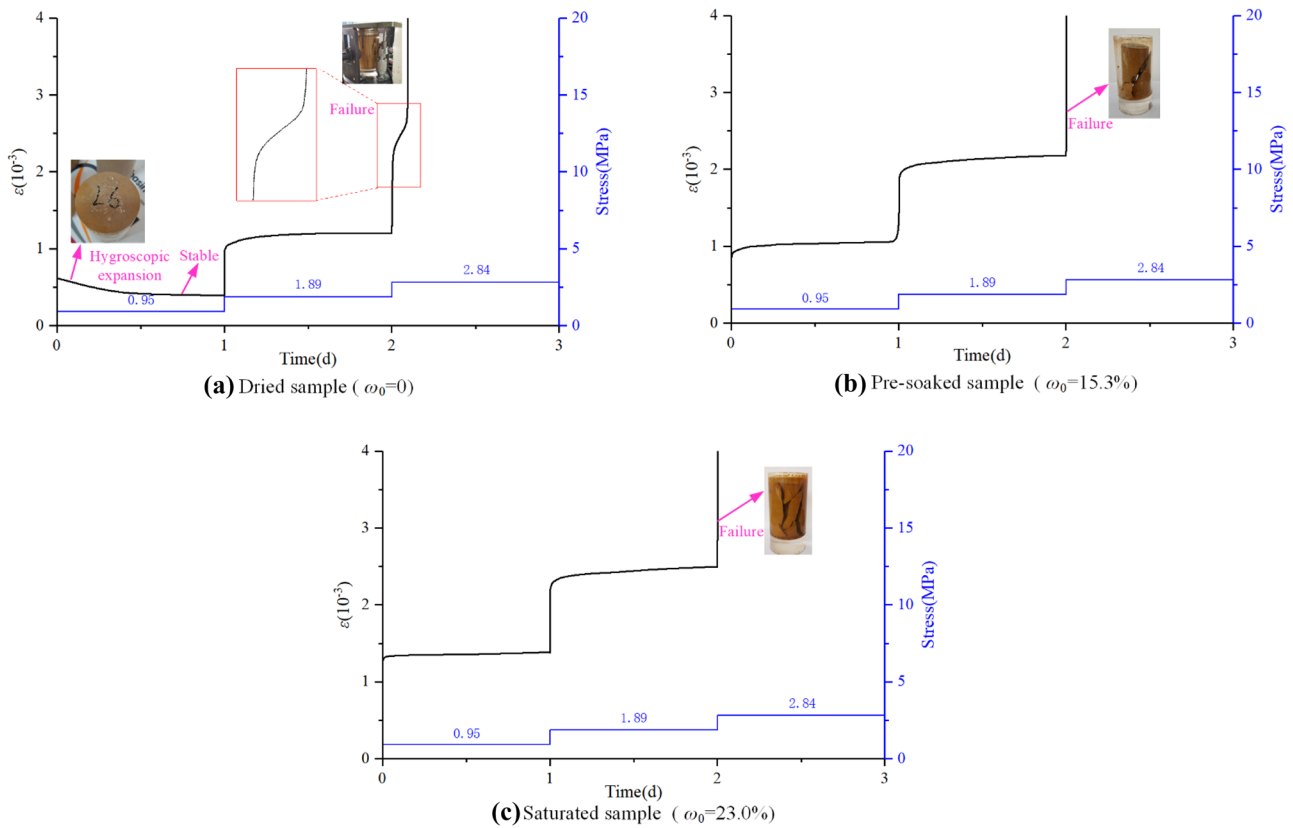


Fig. 7 Creep curves of samples in the soaking condition

means that the deformation of saturated samples is similar under un-soaking and soaking conditions. Consequently, the smaller the initial water content is, the more significant the influence of immersion on the creep deformation. The larger the initial water content is, the more consistent the creep strain of samples in both un-soaking and soaking conditions.

The water content of mudstone increases under soaking conditions. Therefore, it is necessary to obtain the initial water content as well as the water content during the creep test. The water contents are listed in Table 4, where ω_0 represents the initial water content and ω represents the water content during the creep test. As shown in Fig. 4, the water content of the dried sample increases from 0 to 16.4% after immersion in water for 1 h, and then the rate of water absorption decreases. For the sake of simplicity, it can be considered that the ω_0 and ω of the dried sample are 0 and

16.4%, respectively. Analogously, the presoaked sample has high water absorbency after immersion for 1 h. The water content increases from 15.3% to 16.9%. Therefore, the values of ω_0 and ω of the presoaked sample are 15.3% and 16.9%, respectively. The water content of the saturated sample remains constant after immersion, which is 23.0%.

Figure 8 shows the creep curves of three sets of specimens under un-soaking and soaking conditions. As described above, the dried sample exhibits significant expansion deformation under the first stress level, while the water content remains constant under the second stress level. Hence, the creep curve of the specimen under the first stress level is ignored in Fig. 8. In addition, the failure strength and time-to-failure are listed in Table 4.

At the second stress level, the creep curve consists of two stages. Taking the creep curve of the dried sample under the

Table 2 Strains of samples in the soaking condition

Sample	$\sigma = 0.95 \text{ MPa}$				$\sigma = 1.89 \text{ MPa}$				$\sigma = 2.84 \text{ MPa}$			
	ϵ	ϵ_0	ϵ_c	ϵ_c/ϵ	ϵ	ϵ_0	ϵ_c	ϵ_c/ϵ	ϵ	ϵ_0	ϵ_c	ϵ_c/ϵ
Dried	0.40	0.62	-	-	0.81	0.53	0.28	35%	-	1.75	-	-
Presoaked	1.05	0.77	0.28	27%	1.13	0.73	0.40	35%	-	-	-	-
Saturated	1.38	1.22	0.16	12%	1.11	0.70	0.41	37%	-	-	-	-

Table 3 The α values of samples under different stress levels

Sample	$\sigma = 0.95$ MPa	$\sigma = 1.89$ MPa
Dried	-	1.80
Presoaked	1	1.61
Saturated	0.91	1.03

un-soaking conditions as an example, as shown in Fig. 9, in the primary creep stage, the strain increases, while the strain rate decreases. In the steady-state creep stage, the strain is a linear function of time. In particular, the creep rate of this stage is approximately constant, which is called the steady-state creep rate $\dot{\epsilon}$ (Tang et al. 2018).

The value of $\dot{\epsilon}$ is significantly affected by immersion. Table 4 shows that for the samples with the same initial water content, the steady-state creep rate $\dot{\epsilon}$ under soaking conditions is greater than that under un-soaking conditions. For instance, the $\dot{\epsilon}$ values of dried samples under un-soaking conditions and soaking conditions are 0.025 and $0.109 \times 10^{-3}/d$, respectively. If the engineering design is based on the traditional un-soaking condition, the stability of the rock mass is overestimated, which is not conducive to safety. Therefore, considering the creep behavior of rock masses under immersion sheds new light on engineering design.

Water content

As seen from Table 4, the failure strength and time-to-failure of the sample decrease with increasing water content. For the presoaked sample under soaking conditions, the deformation is too large due to the dispersion of the sample. For the other samples, the deformation increases with increasing water content. Moreover, when ω of the samples is the same, the creep deformation is correspondingly the same. For example, the water content of the saturated samples is 23.0% under both un-soaking and soaking conditions. Thus, the failure strength and time-to-failure of the samples in the two conditions are the same, and the creep deformation varies slightly.

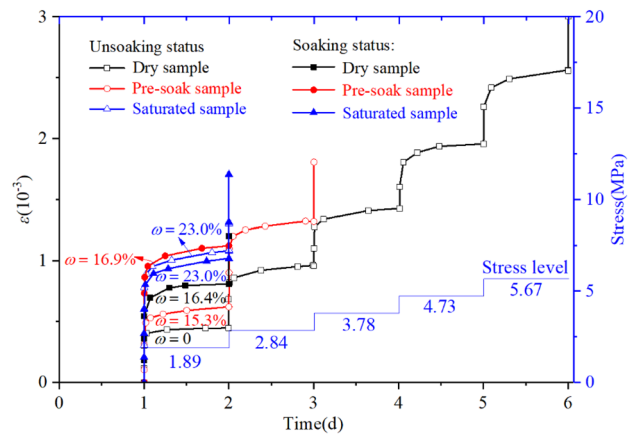


Fig. 8 Creep curve of the samples in the un-soaking and soaking conditions

At the second stress level, the relationship between $\dot{\epsilon}$ and ω is shown in Fig. 10. It can be clearly seen that under the same stress, $\dot{\epsilon}$ increases with increasing water content, and $\dot{\epsilon}$ is equal when ω is the same. For example, the water content of the saturated sample is 23.0% in both un-soaking and soaking conditions, and $\dot{\epsilon}$ is approximately $0.13 \times 10^{-3}/d$ in both conditions. It must also be noted that in Fig. 8, as mentioned before, the creep strain of the presoaked sample is too large under immersion ($\omega = 16.9\%$). Nevertheless, in the steady-state creep stage, $\dot{\epsilon}$ is $0.118 \times 10^{-3}/d$, which is between the $\dot{\epsilon}$ of the dried sample (ω was 16.4%, $\dot{\epsilon}$ was $0.109 \times 10^{-3}/d$) and the $\dot{\epsilon}$ of the saturated sample under soaking conditions (ω was 23.0% and $\dot{\epsilon}$ was $0.13 \times 10^{-3}/d$). Figure 8 also illustrates that $\dot{\epsilon}$ increases with increasing water content.

To investigate the influence of water on the microstructures of mudstone, the scanning electron microscope (SEM) test was conducted. Figure 11 shows the SEM photomicrograph of the dried sample, pre-soaked sample and saturated sample. For the dried sample, the microstructure is compact with few pores. The microstructure is denser than other samples. With increasing water content, the structures become loose and more pores can be observed. For the saturated

Table 4 Water content of the samples and the failure status

Sample	Test condition	$\omega_0(\%)$	$\omega(\%)$	Failure strength (MPa)	Holding time(d)	Steady-state creep rate $\dot{\epsilon}$ ($10^{-3}/d$)
Dried	Un-soaking	0	0	6.62	6	0.025
	Soaking		16.4	2.84	2	0.109
Presoaked	Un-soaking	15.3	15.3	3.78	3	0.088
	Soaking		16.9	2.84	2	0.118
Saturated	Un-soaking	23.0	23.0	2.84	2	0.129
	Soaking		23.0	2.84	2	0.131

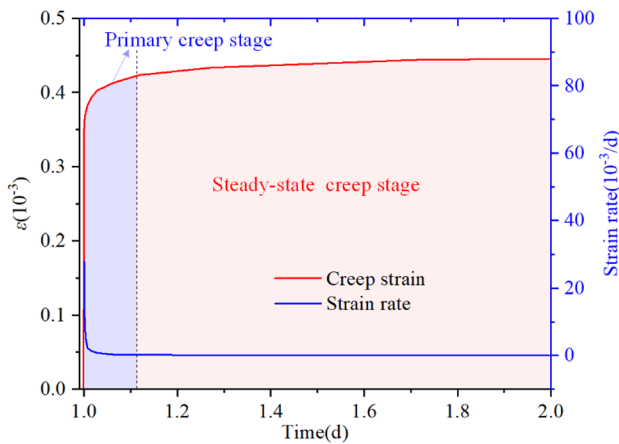


Fig. 9 Two stages of the creep curve

sample, the porosity increases and a large number of crystals are precipitated.

According to the microstructure of mudstone, the degradation mechanism of water on the creep properties can be analyzed. Increasing water contents lead to a looser and more porous microstructure, which further results in reduced cohesion and the degradation of mechanical properties.

Creep constitutive model considering water

Creep constitutive model

During the immersion stage, the creep damage of mudstone can be attributed to the increase in water content. In the constitutive equation, the creep parameters decrease with increasing water content. To further illustrate the effect of water on the creep characteristics of mudstone, an improved

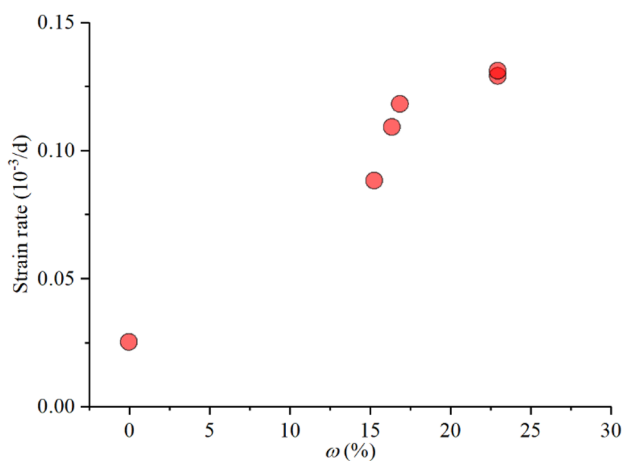


Fig. 10 Relationship between ϵ and ω

creep constitutive model is proposed based on the generalized Kelvin model.

The generalized Kelvin model consists of a Hooke body and a Kelvin body, and its creep constitutive equation is

$$\epsilon = \frac{\sigma_0}{E_M} + \frac{\sigma_0}{E_K} \left(1 - e^{-\frac{E_K}{\eta} t}\right) \tag{2}$$

where σ_0 is the stress, E_M is the instantaneous elastic modulus, E_K is the viscoelastic modulus, and η is the viscosity.

Although the generalized Kelvin model exhibits nonlinear creep characteristics, the linear deformation of two elastic components makes it impossible to describe the nonlinear deformation caused by water damage. Therefore, the generalized Kelvin model is unable to show the relationship between creep parameters and water content. To solve this problem, a creep constitutive model considering water is proposed by introducing damage variables. As shown in Fig. 12, the model consists of a modified Hooke body and a modified Kelvin body. The constitutive equation is

$$\epsilon = \frac{\sigma_0}{E_M(1 - D_{\omega(E_M)})} + \frac{\sigma_0}{E_K(1 - D_{\omega(E_K)})} \left(1 - e^{-\frac{E_K(1 - D_{\omega(E_K)})}{\eta(1 - D_{\omega(E_K)})} t}\right) \tag{3}$$

where D_{ω} is water damage variable.

In light of the damage mechanics theory, there are two methods for defining the damage variables. One definition is based on the effective bearing area in geometric damage. The other definition is derived from the change in the elastic modulus with energy damage. The elastic modulus method is more widely used (Gori et al. 2018) and is applicable to the determination of damage variables in the creep constitutive model considering water (Wang et al. 2019a, Wang et al. 2016, Liu et al. 2014 and Yang et al. 2018). In the second method, the degradation of material properties and the generation of microcracks are considered the main factors of material damage, and the water damage variable is defined as Eq. (4).

$$D_{\omega} = 1 - E_{\omega}/E_0 \tag{4}$$

where E_0 is the initial elastic modulus and E_{ω} is the elastic modulus with water content ω .

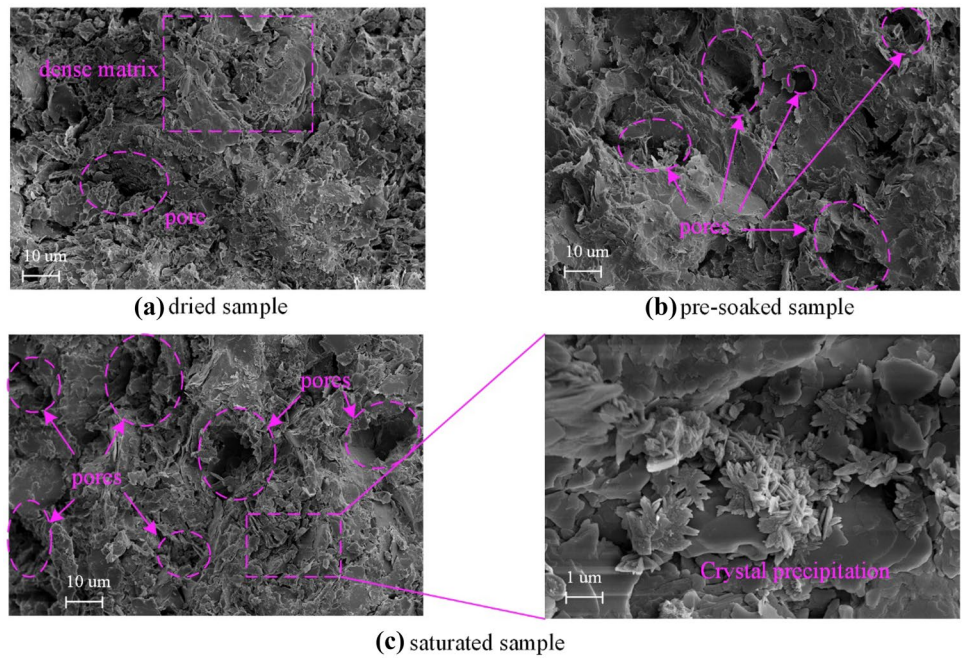
It is generally accepted that there is a linear relationship between the elastic modulus and shear modulus, as shown in Eq. (5).

$$G = \frac{E}{2(1 + \nu)} \tag{5}$$

Creep deformation is usually caused by shear stress. Therefore, the damage variable of the shear modulus is defined based on the second method:

$$D_{\omega}(G) = 1 - G_{\omega}/G_0 \tag{6}$$

Fig. 11 SEM photomicrograph of the mudstones



where $D_\omega(G)$ is the damage variable of the shear modulus, G_0 is the initial shear modulus, and G_ω is the shear modulus with water content ω .

Similarly, the damage variable of viscosity can be given as

$$D_\omega(\eta) = 1 - \eta_\omega/\eta_0 \tag{7}$$

where $D_\omega(\eta)$ is the damage variable of viscosity, η_0 is the initial viscosity, and η_ω is the viscosity with water content ω .

On the basis of the assumption of constant bulk modulus, the one-dimensional creep equation is extended to a three-dimensional equation. The strain tensor consists of a spherical tensor, and the deviatoric strain tensor can be expressed as

$$\epsilon_{ij} = \epsilon_0 \delta_{ij} + e_{ij} \tag{8}$$

where ϵ_0 is the average strain, δ_{ij} is the Kronecker symbol, and e_{ij} is the deviatoric strain tensor.

The relationship between the average strain and stress under the elastic state can be written as

$$\epsilon_0 = \frac{1}{3}(\epsilon_x + \epsilon_y + \epsilon_z) = \frac{1}{3}\epsilon_{kk} \tag{9}$$

$$\epsilon_{kk} = \frac{\sigma_0}{K} = \frac{\sigma_{kk}}{3K} \tag{10}$$

where σ_0 is the average stress and K is the bulk modulus.

The deviatoric stress can be obtained by

$$e_{ij} = \frac{1}{2G} S_{ij} \tag{11}$$

where e_{ij} is the deviatoric stress, G is the shear modulus, and S_{ij} is the deviatoric strain.

In the creep constitutive model considering water,

$$\frac{1}{G} = \frac{1}{G_M^*} + \frac{1}{G_K^*} (1 - e^{-\frac{G_K^*}{\eta^*} t}) \tag{12}$$

where

$$\begin{aligned} G_M^* &= G_M [1 - D_\omega(G_M)] \\ G_K^* &= G_K [1 - D_\omega(G_K)] \\ \eta^* &= \eta [1 - D_\omega(\eta)] \end{aligned} \tag{13}$$

where G_M is the instantaneous shear modulus, G_K is the viscoelastic modulus, and η is the viscosity.

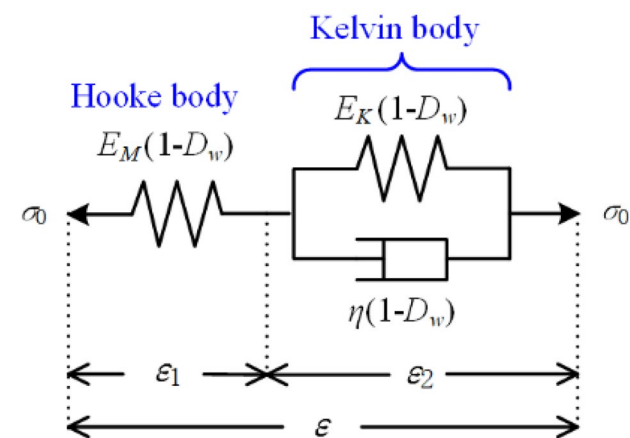


Fig. 12 Creep constitutive model considering water degradation

Table 5 Identification values of the creep parameters

Sample	Test condition	G_M (MPa)	G_K (MPa)	η (MPa·s)
Dried	un-soaking	1.00	1.30	3419.57
	soaking	0.70	0.80	1080.00
Presoaked	un-soaking	0.70	0.84	1260.00
	soaking	0.66	0.70	972.00
Saturated	un-soaking	0.44	0.55	108.00
	soaking	0.50	0.55	108.00

Consequently, the three-dimensional constitutive model considering creep degradation can be expressed as follows:

$$\epsilon_{ij} = \frac{\sigma_{kk}}{9K} \delta_{ij} + \left[\frac{1}{2G_M^*} + \frac{1}{2G_K^*} \left(1 - e^{-\frac{G_K^*}{\eta^*} t} \right) \right] S_{ij} \quad (14)$$

Relationship between water and creep parameters

The nonlinear least square method is used for the parameter identification of creep curves. This method has the advantages of fast convergence, high accuracy and little dependence on the initial value of the iteration. The creep parameters of the three sets of specimens under soaking and un-soaking conditions are identified. The results are shown in Table 5.

The relationship between the creep parameters and water content is shown in Fig. 13. The values of G_M , G_K and η decrease linearly with increasing water content, as shown in Eq. (15).

$$\begin{aligned} G_M &= 1.02812 - 0.0229\omega \\ G_K &= 1.26926 - 0.03082\omega \\ \eta &= 3429.03785 - 144.04502\omega \end{aligned} \quad (15)$$

Substituting Eq. (15) into Eqs. (6) and (7), the damage evolution equation of the creep parameter is obtained:

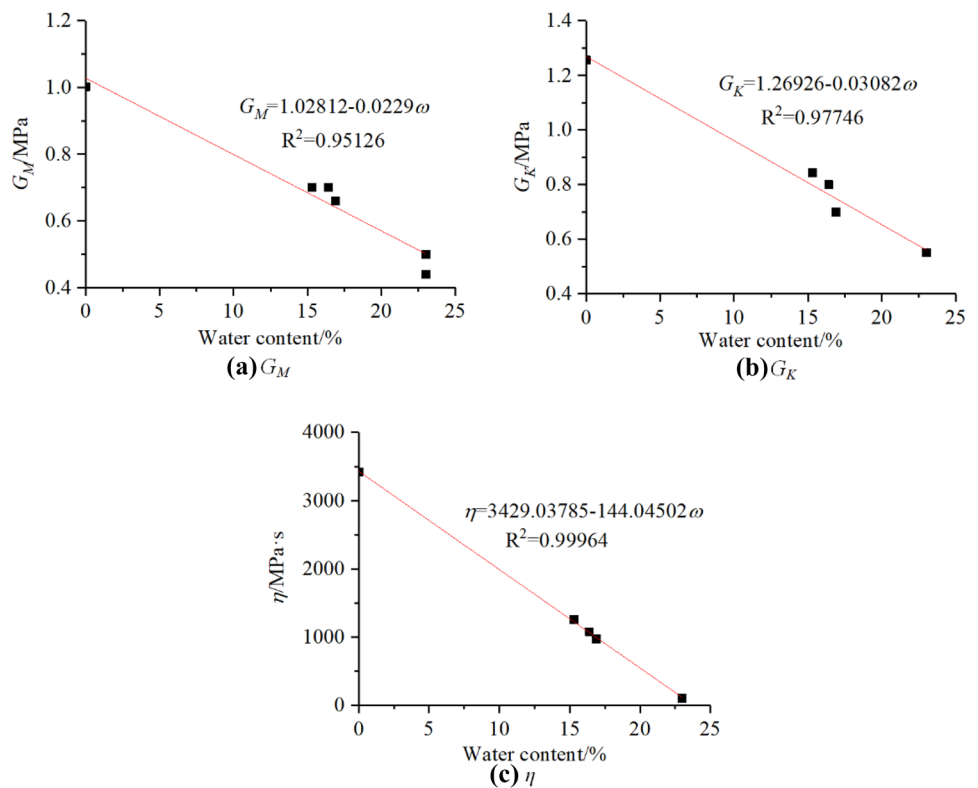
$$\begin{aligned} D_\omega(G_M) &= 0.024282\omega \\ D_\omega(G_K) &= 0.022274\omega \\ D_\omega(\eta) &= 0.042007\omega \end{aligned} \quad (16)$$

Verification

Uniaxial creep test

The creep constitutive model is incorporated into FLAC^{3D} by writing a FISH function. To verify the proposed creep constitutive model, a serious numerical creep test under un-soaking and soaking conditions is carried out. As shown in Fig. 14, the numerical model is cylindrical, 50

Fig. 13 Relationship between creep parameters and water content during the creep test



mm in diameter and 100 mm in height, which is the same as the mudstone samples used in the laboratory test. The bottom of the model is fixed, and a uniformly distributed load is applied to the top of the model.

The numerical simulation is carried out using the Burgers model, which is a built-in model in FLAC^{3D}. Since no value is assigned to the property “mviscosity,” the Maxwell dashpot is not taken into account by the model (Itasca 2003). In this way, the Burgers model degenerates into a generalized Kelvin model. The properties of the model are as follows: density $\rho = 2000 \text{ kg/m}^3$ and bulk modulus $K = 1 \times 10^9 \text{ Pa}$. The values of G_M , G_K and η are determined according to Table 5 when the water content is 0. These creep parameters decrease with increasing water content. Figure 15 shows a flowchart of the approach for the numerical experiments that were conducted in this study.

Results

Comparisons of the creep curves obtained by numerical simulation and the laboratory test are shown in Figs. 16 and 17. It should be noted that the emphasis of this study is the deformation characteristics of rock masses considering water. Therefore, the hygroscopic expansion of the rock sample is not taken into consideration in the numerical simulation, as shown in Fig. 17a.

The simulation results are in good agreement with the laboratory test results. The simulation results highlight that the creep deformation increases with increasing water content, as do the laboratory test results. The deformation law of the simulated and test results is similar despite the slight deviation, which verifies the correctness of the

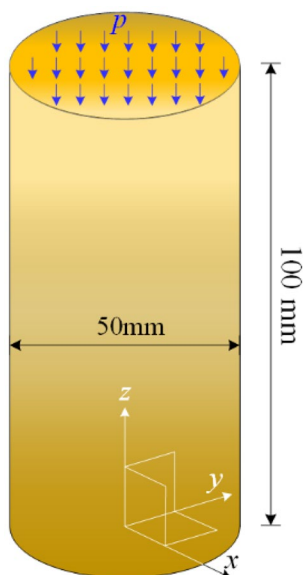


Fig. 14 Numerical model of the uniaxial creep test

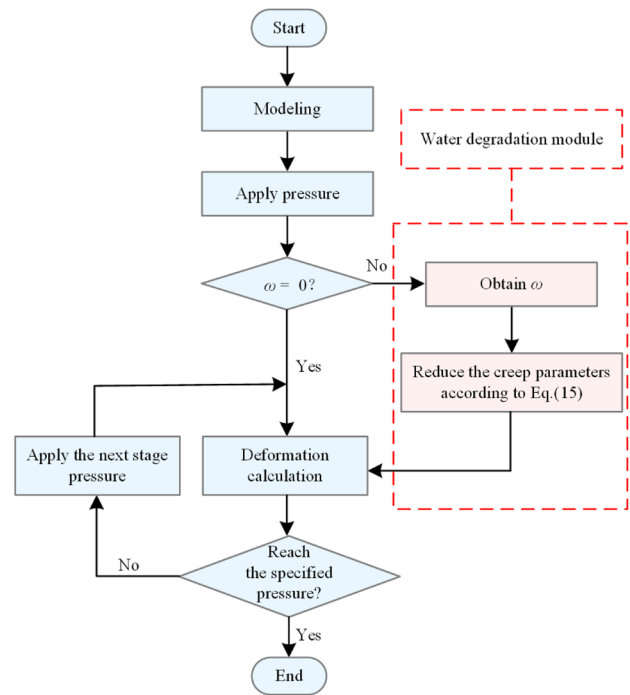


Fig. 15 Flowchart of multistage creep test in FLAC^{3D}

model, as well as the selection of parameters. The results indicate that the proposed model is capable of simulating the creep behavior of rock masses under soaking conditions.

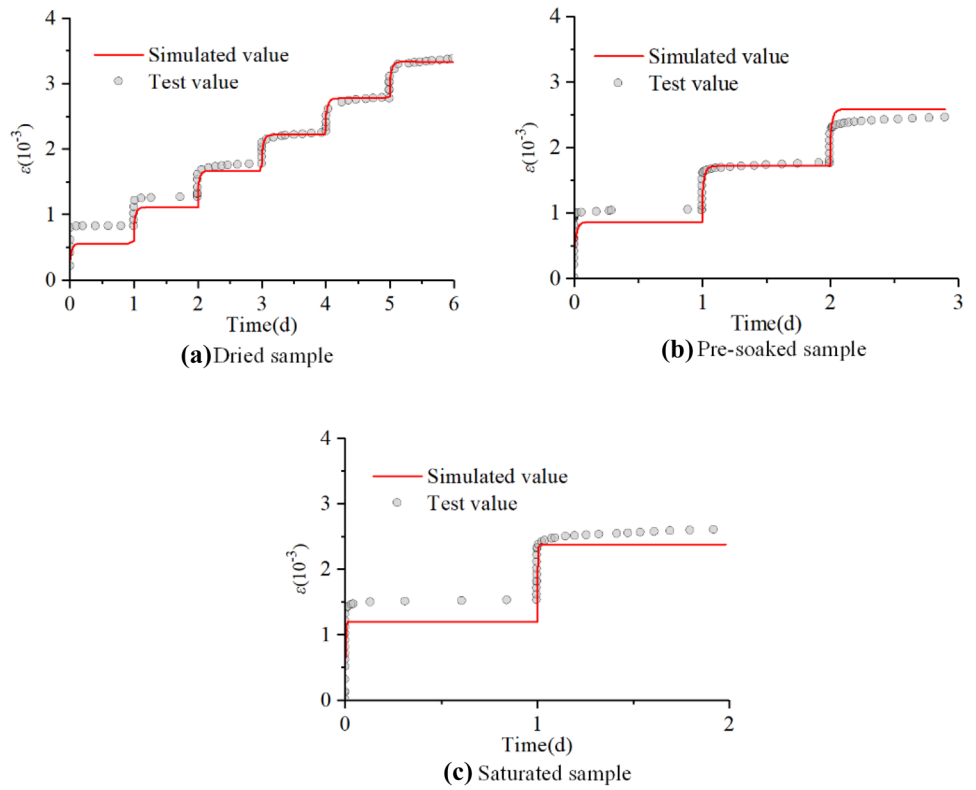
Moreover, a comparison of the proposed model and previous study was made. Creep damage models under water containing conditions were studied by Yang et al. (2018) and Liu et al. (2014). A variable-parameter creep damage model that considers the effects of dry–wet cycling on granite is proposed and verified by Zhang et al. (2021). It is seen that the creep parameters decrease with increasing water contents or the number of drying–wetting cycles. Consequently, the rationality of the creep damage model in this paper can be validated by these previous studies. The long-term deformation of the rock in the hydro-fluctuation belt was influenced by the water contents and soaking conditions. Therefore, the creep damage model in this paper is suitable for routine engineering practice.

Simulation of long-term deformation of the Majiagou landslide

Project description

As shown in Fig. 18, the Majiagou landslide, situated on the left bank of the Zhaxi River in the Three Gorges Reservoir

Fig. 16 Comparison of the simulated and test values in the un-soaking condition



(He et al. 2020), is selected to study the long-term deformation of the slope after impoundment. The toe and crown of this landslide are at elevations of 124 m and 284 m,

respectively. The average slope of the Majiagou landslide is 15°, and the sliding direction of the landslide is almost perpendicular to the Zhaxi River (Ma et al. 2017).

Fig. 17 Comparison of the simulated and test values in the soaking condition

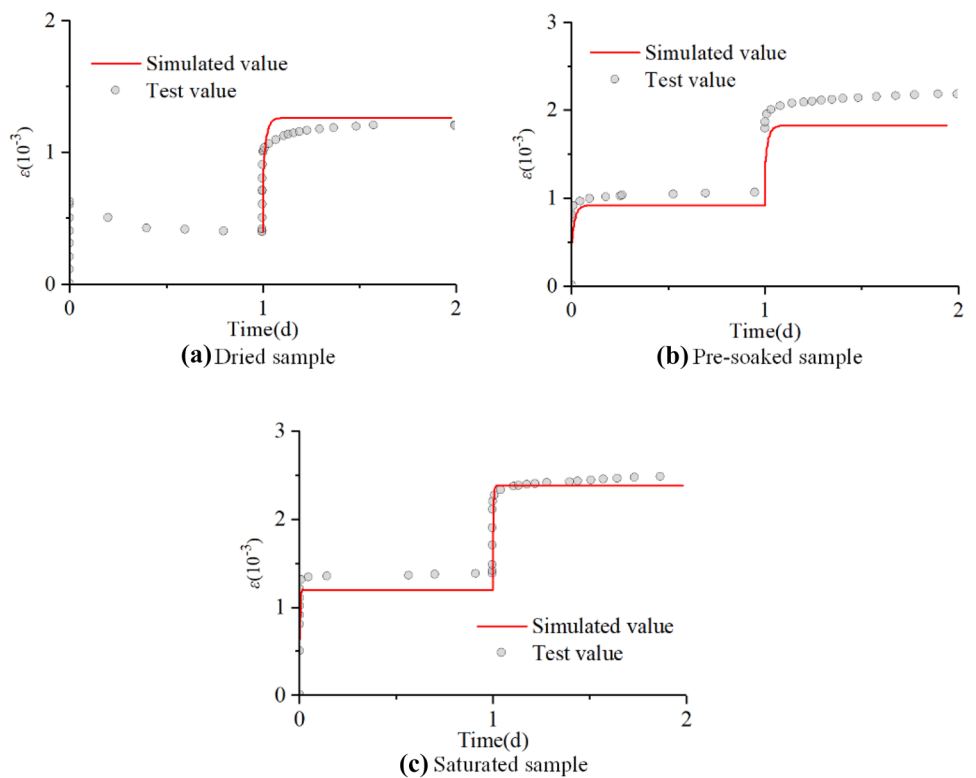
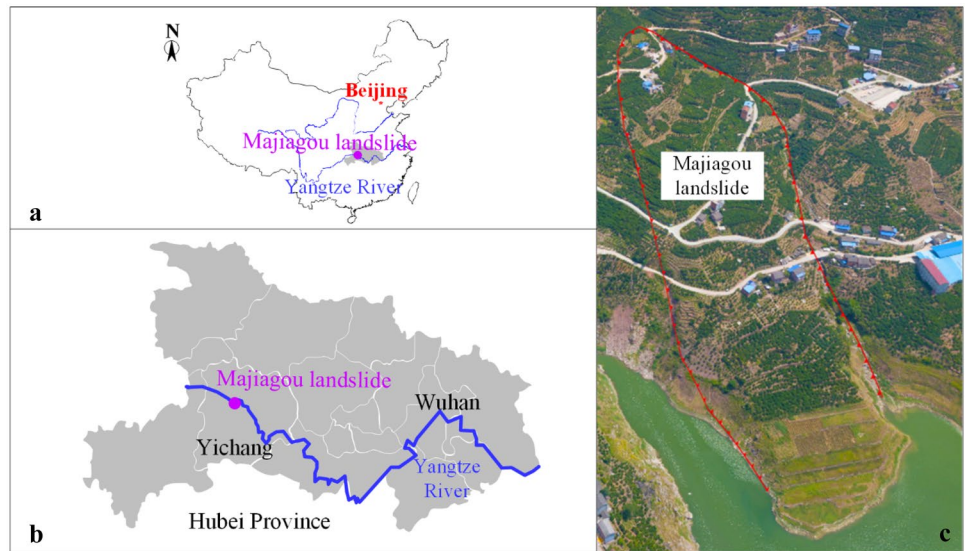


Fig. 18 The Majiagou landslide in the Three Gorges Reservoir area. **a** and **b** show the location of the Majiagou landslide in the Hubei province; **c** is a top view of the Majiagou landslide



The profile of the Majiagou landslide is shown in Fig. 19. The bedrock is weathered interbedded argillaceous siltstone and silty mudstone of the Jurassic Suining Formation with low permeability. The surficial deposits consist of gravel mixed with silty clay. The mudstone could easily be softened by water (Zhou et al. 2020). The deformation of the landslide was observed after the first impoundment of the reservoir in 2003. During the monitoring period between 2007 and 2009, GPS monitoring station G01 recorded the largest average annual deformation at approximately 183 mm/year (Zhang et al. 2018).

Modeling and simulation methods

Based on the fluid–solid interaction method of FLAC^{3D}, the creep deformation of the Majiagou landslide after impoundment was simulated. The FLAC^{3D} model of the Majiagou landslide is depicted in Fig. 20, which is divided into 543 elements and 1180 nodes. The horizontal distance of the model is 550 m, and the elevation of the back edge is 284 m.

In the numerical model of the Majiagou landslide, gravitational field is the main component of stress field. The boundary condition of the model was set as the displacement fixed boundary. The top surface of slope was set as free boundary, and the normal displacement constraint was applied on the bottom and four vertical surfaces. Head-dependent flow boundaries were used to quantify flow in of the model domain. The hydro-mechanical coupling method was used and the water level was set as 145 m and 175 m. G01 and G02 were taken as the observation points. The elevations of the two observation points are 200 m and 227 m. The rock mass is divided into three groups: bedrock, deformed rock mass and superficial deposits. The creep constitutive model considering water is adopted for all three groups. The physical and mechanical parameters of each group are determined by geological data and inversion (Zhang et al. 2018; Hu et al. 2019), as listed in Table 6.

The range of the creep parameters (G_M , G_K and η) is first determined according to the engineering cases (Shao et al. 2003; Zhang et al. 2015; Zhou et al. 2011). Then, the creep parameters are calibrated by the measured displacement of

Fig. 19 Profile of the Majiagou landslide

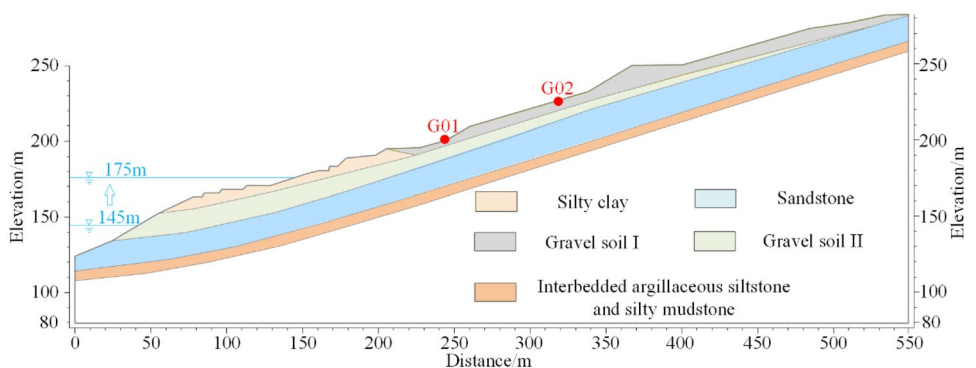
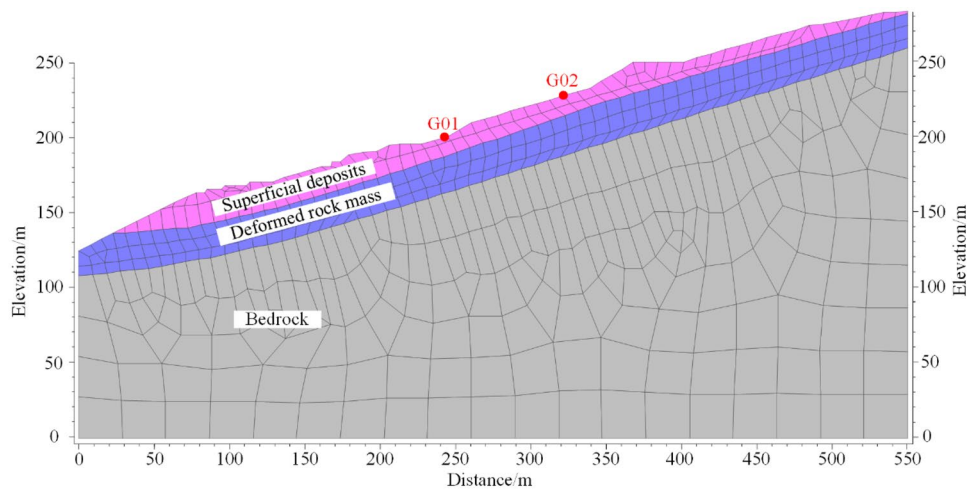


Fig. 20 Numerical model of the Majiagou landslide



the landslide from August to December 2008. The creep parameters are taken as the optimization variables, and the objective function is to minimize the residual sum of squares between the calculated displacement and the measured displacement. By modifying the value of the creep parameters gradually and evaluating the objective function of each group of creep parameters, the iteration can be stopped when the objective function obtains the minimal value, and the creep parameters here are at their optimal values (Shao et al. 2003). Table 6 shows the creep parameters obtained according to the above steps. In addition, the values of damage variables $D_\omega(G_M)$, $D_\omega(G_K)$ and $D_\omega(\eta)$ are 6ω , 6ω and $(10^{-27})^\omega$, respectively.

In accordance with the monitoring data (Zhang et al. 2018), the water level of 145 m will be remained till October 2008 when it starts to increase to 175 m. Then, the water level starts to decrease gradually from 175 to 145 m in January 2009. The decline in the reservoir water level results in different water contents of rock mass in hydro-fluctuation belt. When impounding again, the rock mass containing different water contents in hydro-fluctuation belt will deform under soaking conditions. This process is implemented in FLAC^{3D} by the following steps. First, the seepage field of the landslide under water levels of 145 m and 175 m is calculated. Then, it is considered that during the impoundment process, the characteristics of the blocks deteriorate, and

the creep parameters are reduced accordingly. Finally, the calculation results are obtained.

Simulation results

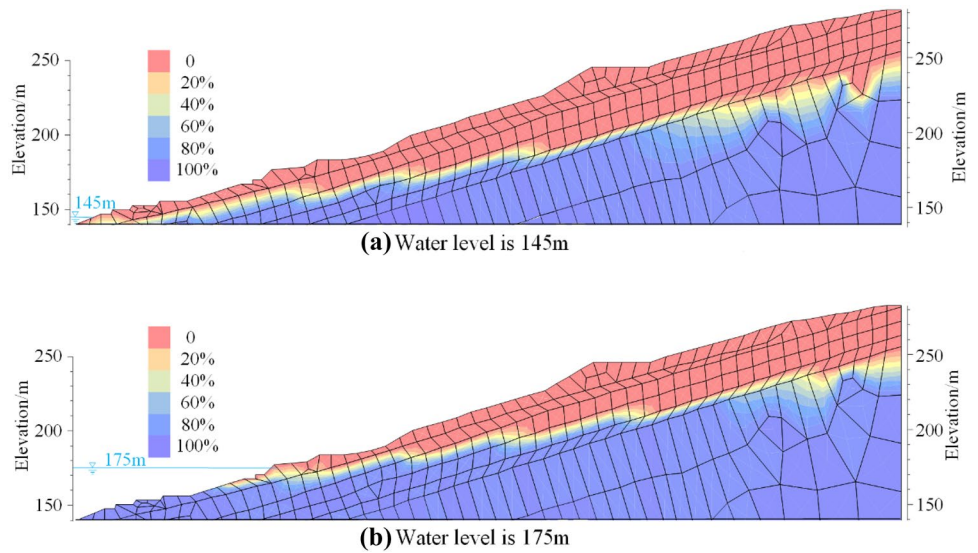
Figure 21 shows the saturation nephrograms of the Majiagou landslide under water levels of 145 m and 175 m. For the blocks between elevations of 145–175 m, the saturation is relatively low before impoundment. However, the saturation increases significantly after impoundment. The rock mass in the hydro-fluctuation belt is almost saturated. It is noted that the saturation of rock mass at high elevations is not affected by water impoundment.

Figure 22 shows the X-direction displacement nephrogram of the Majiagou landslide under water levels of 145 m and 175 m. When the water level is 145 m, the displacement of rock mass in the hydro-fluctuation belt is less than 52 mm. The displacement of rock mass in the hydro-fluctuation belt increased to 200 mm when the water level increased to 175 m, which is almost 4 times that before impoundment. While the displacement of rock mass at high elevation changed little, the increase in the reservoir water level leads to the increase in the saturation of rock mass, which further results in an increase in deformation.

Table 6 Values of parameters

Group	Density ρ (kg/m ³)	Bulk modulus K (Pa)	Permeability coefficient (cm/s)	G_M (MPa)	G_K (MPa)	η (MPa·s)
Bedrock	2500	7.5×10^8	10^{-4}	600	400	4.4×10^9
Deformed rock mass	2450	5.8×10^7	3×10^{-4}	600	400	4.4×10^9
Superficial deposits	2110	9.3×10^6	6×10^{-4}	30	20	6.4×10^9

Fig. 21 Saturation nephrogram under different water levels



In addition, the creep curves of monitoring points and the relationship between creep rate and time are shown in Fig. 23. The numerical simulation results of G01 show that in the calibration interval, that is, from August to December 2008, the displacement increases slowly, and the maximum creep rate is 0.3 mm/d. Affected by the rise in the water level, the creep rate increases significantly, and the maximum rate is 10.4 mm/d after October. The deformation of G01 is 63 mm within the calculation interval. The creep curve of G02 shows similar long-term deformation characteristics. The deformation of G02 is 41 mm within the calculation interval, which is less than that of G01.

The deformation prediction interval begins after December 2008. In this interval, the predicted creep curve from December 2008 to February 2009 is obtained using the calibrated parameters. The results show that both the displacement and the creep rate are in good agreement with the measured values, which further substantiates that the creep constitutive model considering water is suitable for simulating the long-term deformation of reservoir slopes after impoundment. Most importantly, the results emphasize that an increase in the water level results in an increase in the water content of the rock mass, which further causes creep damage and then leads to an increase in the deformation and creep rate.

Fig. 22 X-direction displacement nephrogram under different water levels

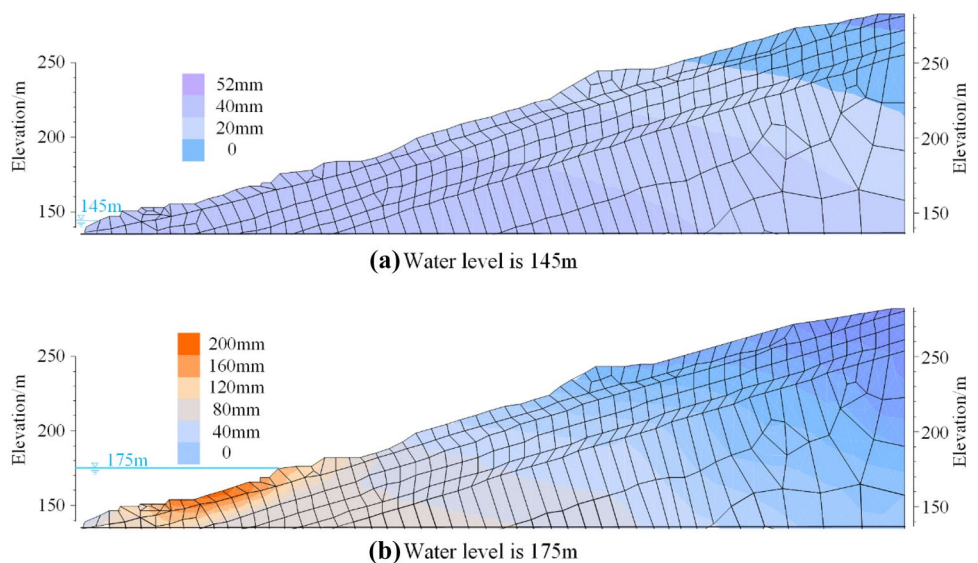
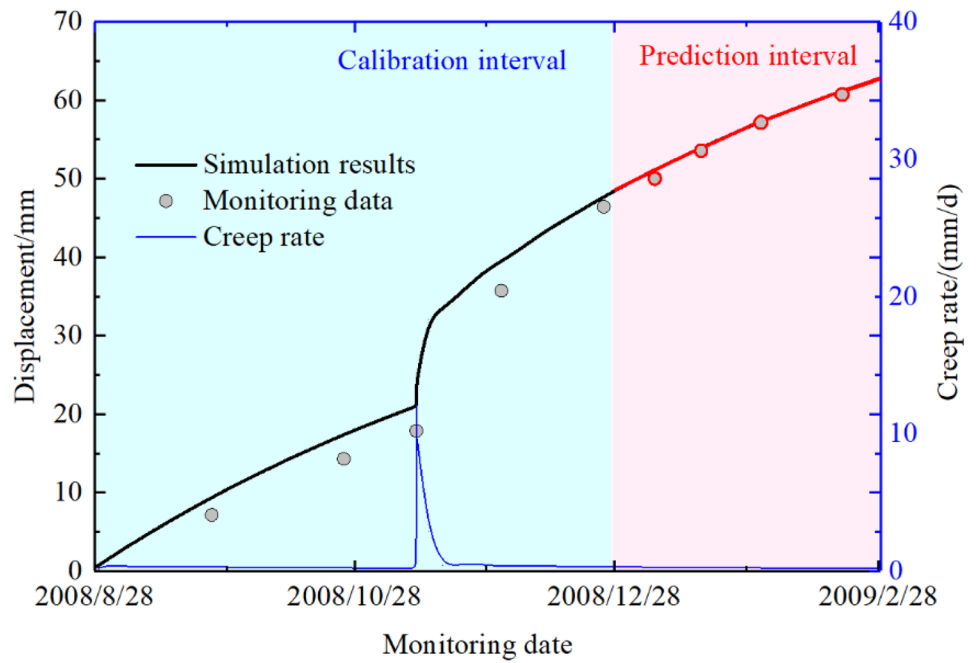
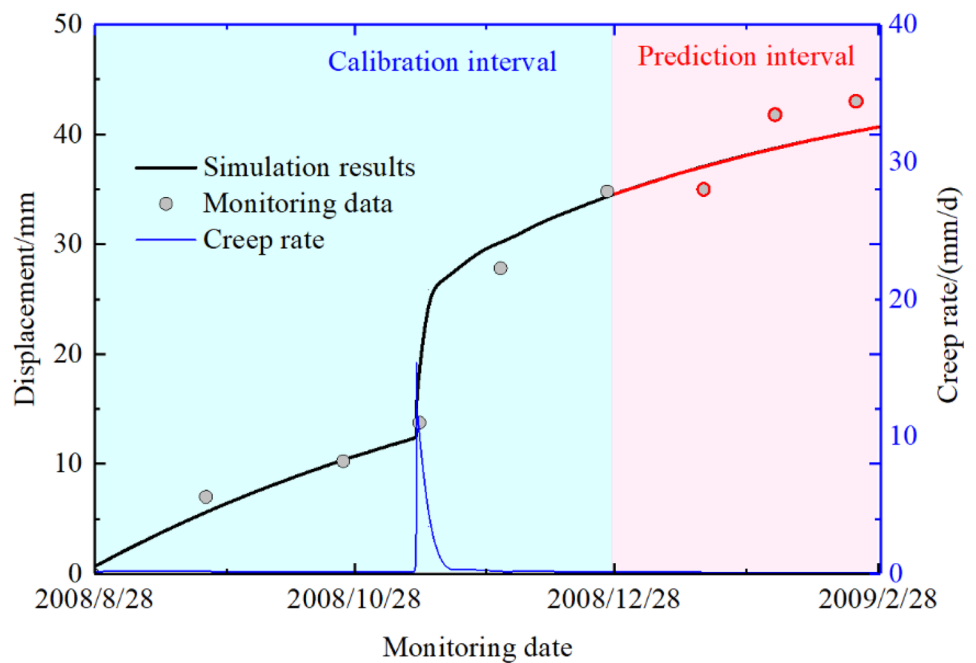


Fig. 23 Creep curves of the monitoring points



(a) G01



(b) G02

Conclusions and discussion

In this study, multistage creep tests of mudstones with different initial water contents are carried out under un-soaking and soaking conditions. An improved creep

constitutive model considering water is proposed, and the long-term deformation of the reservoir bank after impoundment is simulated using the proposed constitutive model. The main conclusions are as follows:

1. Under the un-soaking condition, the strength of the mudstone decreases and the axial strain and the proportion of creep strain in the total strain increase with increasing initial water content.
2. The influence of soaking conditions on the strength, creep strain and the steady-state creep rate of the mudstone was verified. For the unsaturated samples, the strength and deformation under un-soaking conditions are not greater than those under soaking conditions. In addition, the creep behavior of saturated samples in un-soaking and soaking conditions is similar. Moreover, the steady-state creep rate of the samples increases significantly under immersion. It is necessary for engineering safety to consider the creep damage characteristics of the rock mass after impoundment.
3. The degradation of the creep characteristics of mudstone is mainly affected by the water content ω during the creep test. The failure strength and time-to-failure of the samples decrease with increasing ω , while the creep strain and steady-state creep rate increase. The creep behavior is consistent when the ω of the samples is the same. In other words, the creep parameters are a function of the water content.
4. According to the degradation of creep parameters and the damage evolution equation, a creep constitutive model considering water is proposed and incorporated into the FLAC^{3D} software. Additionally, this model is verified by comparing a series of simulation results with laboratory creep tests.
5. The long-term deformation of the Majiagou landslide after impoundment is simulated using the proposed constitutive model. The creep curve of typical measuring points obtained by simulation agrees well with the measured value, indicating the effectiveness of the constitutive model. The simulation results reveal the deformation mechanism of the landslide in the rising stage.

It is noted that the experiments in this study are all carried out under free absorption conditions, and the effects of confining pressure and seepage pressure are not taken into consideration, which is a topic of future works. Moreover, in the condition of reservoir water level fluctuation, immersion-air dry circulation may lead to cumulative fatigue damage of rock. Consequently, the chemical composition and secondary porosity of the rock mass change, and the influencing factors of creep degradation are more complicated and need to be further elucidated.

Funding The work reported in this paper has received financial support from National Natural Science Foundation of China (No.51879127), National Key R&D Program of China (nos.2019YFC0605001), National Key R&D Program of China (No.2018YFC1505005), National Natural Science Foundation of China (No.51769014, 42077253) and Natural

Science Foundation of Hubei Province (No. 2016CFA083). These supports are gratefully acknowledged.

Declarations

Conflict of interests The authors declare that they have no known competing financial interests or personal relationships that could have appeared to influence the work reported in this paper.

References

- Brijes M, Priyesh V (2015) Uniaxial and triaxial single and multi-stage creep tests on coal-measure shale rocks. *Int J Coal Geol* 137(1):55–65. <https://doi.org/10.1016/j.coal.2014.11.005>
- Deng HF, Zhou ML, Li JL, Sun XS, Huang YL (2016) Creep degradation mechanism by water-rock interaction in the red-layer soft rock. *Arab J Geosci* 9(12):601. <https://doi.org/10.1007/s12517-016-2604-6>
- Doi N, Kato T, Kubo T, Noda M, Shiraishi R, Suzuki A et al (2014) Creep behavior during the eutectoid transformation of albite: Implications for the slab deformation in the lower mantle. *Earth Planet Sci Lett* 388:92–97. <https://doi.org/10.1016/j.epsl.2013.09.009>
- Ghorbani M, Sharifzadeh M (2009) Long term stability assessment of Siah Bisheh powerhouse cavern based on displacement back analysis method. *Tunn Undergr Space Technol* 24(5):574–583. <https://doi.org/10.1016/j.tust.2009.02.007>
- Gori L, Penna SSP, Pitangueira RLDS (2018) Discontinuous failure in micropolar elastic-degrading models. *Int J Damage Mech* 27(10):1482–1515
- Hashiba K, Fukui K (2016) Time-dependent behaviors of granite: loading-rate dependence, creep, and relaxation. *Rock Mech Rock Eng* 49(7):2569–2580. <https://doi.org/10.1007/s00603-016-0952-x>
- Hashiba K, Fukui K, Kataoka M, Chu SY (2018) Effect of water on the strength and creep lifetime of andesite. *Int J Rock Mech Min Sci* 108:37–42. <https://doi.org/10.1016/j.ijrmms.2018.05.006>
- He CC, Hu XL, Tannant DD, Tan FL, Zhang YM, Zhang H (2018) Response of a landslide to reservoir impoundment in model tests. *Eng Geol* 247:84–93. <https://doi.org/10.1016/j.enggeo.2018.10.021>
- He CC, Hu XL, Xu C, Wu SS, Liu C (2020) Model test of the influence of cyclic water level fluctuations on a landslide. *J Mt Sci Engl* 17(1):191–202. <https://doi.org/10.1007/s11629-019-5713-9>
- Herrmann J, Rybacki E, Sone H, Dresen G (2019) Deformation experiments on bowland and posidonia shale—part II: creep behavior at in situ p_c - T conditions. *Rock Mech Rock Eng* 53(2):755–779. <https://doi.org/10.1007/s00603-019-01941-2>
- Hu XL, Tang HM, Li CD, Sun RX (2012) Stability of Huangtupo riverside slumping mass II# under water level fluctuation of Three Gorges Reservoir. *J Earth Sci* 23:326–334. <https://doi.org/10.1007/s12583-012-0259-0>
- Hu XL, Zhou C, Xu C, Liu DZ, Wu SS, Li L (2019) Model tests of the response of landslide-stabilizing piles to piles with different stiffness. *Landslides* 16(125):2187–2200. <https://doi.org/10.1007/s10346-019-01233-4>
- Huang D, Luo SL, Zhong Z, Gu DM, Song YX, Tomás R (2020) Analysis and modeling of the combined effects of hydrological factors on a reservoir bank slope in the Three Gorges Reservoir area. *China Eng Geol*. <https://doi.org/10.1016/j.enggeo.2020.105858>
- Itasca (2003) Fast Lagrangian analysis of continua in 3 dimensions, user's manual. Itasca Consulting Group Inc, Minneapolis, Minnesota (Group IC editor)

- Jia GW, Zhan T, Chen YM et al (2009) Performance of a large-scale slope model subjected to rising and lowering water levels. *Eng Geol* 106(1–2):92–103. <https://doi.org/10.1016/j.enggeo.2009.03.003>
- Jiang J, Ehret D, Wei X et al (2011) Numerical simulation of Qiaotou Landslide deformation caused by drawdown of the Three Gorges Reservoir, China. *Environ Earth Sci* 62(2):411–419. <https://doi.org/10.1007/s12665-010-0536-0>
- Kumagai N, Ito H, Sasajima S (1986) Long-term creep of rocks—experimental results with large specimens obtained in 27 years and those with small specimens in 10 years. *J Soc Mater Sci Japan* 35(392):484–489. <https://doi.org/10.2472/jsms.35.484>
- Liu L, Wang GM, Chen JH, Yang S (2013) Creep experiment and rheological model of deep saturated rock. *T Nonferr Metal Soc China* 23(2):478–483. [https://doi.org/10.1016/s1003-6326\(13\)62488-7](https://doi.org/10.1016/s1003-6326(13)62488-7)
- Liu X, Wang T, Wang J (2014) Creep model of low-grade metamorphic slate considering moisture degradation effect. *Chin J Rock Mech Eng* 33(12):2384–2389. <https://doi.org/10.13722/j.cnki.jrme.2014.12.002>
- Liu Y, Liu CW, Kang YM, Wang D, Ye DY (2015) Experimental research on creep properties of limestone under fluid–solid coupling. *Environ Earth Sci* 73(11):7011–7018. <https://doi.org/10.1007/s12665-015-4022-6>
- Lu YL, Wang LG (2017) Effect of water and temperature on short-term and creep mechanical behaviors of coal measures mudstone. *Environ Earth Sci* 76(17):597. <https://doi.org/10.1007/s12665-017-6941-x>
- Ma JW, Tang HM, Hu XL, Bobet A, Zhang M, Zhu TW et al (2017) Identification of causal factors for the Majiagou landslide using modern data mining methods. *Landslides* 14(1):311–312. <https://doi.org/10.1007/s10346-016-0693-7>
- Pablo IJ, Hatzor YH (2018) Rapid sliding and friction degradation: Lessons from the catastrophic Vajont landslide. *Eng Geol* 244:96–106. <https://doi.org/10.1016/j.enggeo.2018.07.029>
- Shao JF, Zhu QZ, Su K (2003) Modeling of creep in rock materials in terms of material degradation. *Comput Geotech* 30(7):549–555. [https://doi.org/10.1016/S0266-352X\(03\)00063-6](https://doi.org/10.1016/S0266-352X(03)00063-6)
- Ston J, Scrivener K (2019) Basic creep of limestone–calcined clay cements: An experimental and numerical approach. *Theor Appl Fract Mec*. <https://doi.org/10.1016/j.tafmec.2019.102270>
- Tang SB, Yu CY, Heap MJ, Chen P (2018) The influence of water saturation on the short- and long-term mechanical behavior of red sandstone. *Rock Mech Rock Eng* 51(9):2669–2687. <https://doi.org/10.1007/s00603-018-1492-3>
- Urai JL, Spiers CJ, Zwart HJ, Lister GSJN (1986) Weakening of rock salt by water during long-term creep. *Nature* 324(6097):554–557. <https://doi.org/10.1038/324554a0>
- Wang HB, Xu WY, Xu RC, Jiang QH, Liu JH (2007) Hazard assessment by 3D stability analysis of landslides due to reservoir impounding. *Landslides* 4(4):381–388. <https://doi.org/10.1007/s10346-007-0095-y>
- Wang JB, Zhang Q, Song ZP, Zhang YW (2019a) Creep properties and damage constitutive model of salt rock under uniaxial compression. *Int J Damage Mech* 29(6):902–922. <https://doi.org/10.1177/1056789519891768>
- Wang QY, Zhu WC, Xu T, Niu LL (2016) Numerical simulation of rock creep behavior with a damage-based constitutive law. *Int J Geomech* 17(1):04016044. [https://doi.org/10.1061/\(ASCE\)GM.1943-5622.0000707](https://doi.org/10.1061/(ASCE)GM.1943-5622.0000707)
- Wang YY, Wang H, Shi X (2019b) Creep Investigation on Shale-Like Material with Preexisting Fissure under Coupling Temperatures and Confining Pressures. *Adv Civ Eng* 11:1–10. <https://doi.org/10.1155/2019/7861305>
- Xiong LX, Li TB, Yang LD (2014) Biaxial compression creep test on green-schist considering the effects of water content and anisotropy. *KSCE J Civ Eng* 18(1):103–112. <https://doi.org/10.1007/s12205-014-0276-x>
- Yang C, Daemen J, Yin JH (1999) Experimental investigation of creep behavior of salt rock. *Int J Rock Mech Min Sci* 36(2):233–242. [https://doi.org/10.1016/S0148-9062\(98\)00187-9](https://doi.org/10.1016/S0148-9062(98)00187-9)
- Yang CH, Daemen JJK (1997) Temperature effects on creep of tuff and its time-dependent damage analysis. *Int J Rock Mech Min Sci* 34:345.e1–345.e12. [https://doi.org/10.1016/S1365-1609\(97\)00203-7](https://doi.org/10.1016/S1365-1609(97)00203-7)
- Yang HF, Jian WX, Wang FW, Meng FH, Okeke AC (2013) Numerical Simulation of Failure Process of the Qianjiangping Landslide Triggered by Water Level Rise and Rainfall in the Three Gorges Reservoir, China. *Progress of Geo-disaster mitigation technology in Asia, Environmental Science and Engineering*. Springer, Berlin, Heidelberg, pp 503–523. https://doi.org/10.1007/978-3-642-29107-4_29
- Yang XJ, Wang JM, Zhu C, He M (2019) Effect of Water on Long-Term Strength of Column Rocks Based on Creep Behavior in Yungang Grottoes. *China Geotech Geol Eng*. <https://doi.org/10.1007/s10706-018-0601-0>
- Yang XR, Jiang AN, Jiang ZB (2018) Creep test and damage model of soft rock under water containing condition. *Rock Soil Mech* 39:167–174. <https://doi.org/10.16285/j.rsm.2017.2560>
- Yu CY, Tang SB, Tang CA, Duan D, Zhang YJ, Liang ZZ, Ma K, Ma TH (2019) The effect of water on the creep behavior of red sandstone. *Eng Geol* 253:64–74. <https://doi.org/10.1016/j.enggeo.2019.03.016>
- Zhang F, Jiang A, Yang X (2021) Shear creep experiments and modeling of granite under dry-wet cycling. *Bull Eng Geol Environ* 80:5897–5908. <https://doi.org/10.1007/s10064-021-02282-7>
- Zhang Y, Xu WY, Shao JF, Zhao HB, Wei W (2015) Experimental investigation of creep behavior of elastic rock in Xiangjiaba Hydropower Project. *Water Sci Eng* 8(1):55–62. <https://doi.org/10.1016/j.wse.2015.01.005>
- Zhang YM, Hu XL, Tannant DD, Zhang GC, Tan FL (2018) Field monitoring and deformation characteristics of a landslide with piles in the Three Gorges Reservoir area. *Landslides* 15(5):581–592. <https://doi.org/10.1007/s10346-018-0945-9>
- Zhao B, Liu D, Dong Q (2011) Experimental research on creep behaviors of sandstone under uniaxial compressive and tensile stresses. *J Rock Mech Geotech Eng* 3(suppl1):438–444. <https://doi.org/10.3724/SP.J.1235.2011.00438>
- Zhou C, Hu XL, Zheng WB, Xu C, Wang Q (2020) Displacement characteristic of landslides reinforced with flexible piles: field and physical model test. *J Mt Sci Engl* 17(4):787–800. <https://doi.org/10.1007/s11629-019-5743-x>
- Zhou HW, Wang CP, Han BB, Duan ZQ (2011) A creep constitutive model for salt rock based on fractional derivatives. *Int J Rock Mech Min Sci* 48(1):116–121. <https://doi.org/10.1016/j.jrmm.2010.11.004>
- Zhou ZL, Cai X, Cao WZ, Li XB, Xiong C (2016) Influence of water content on mechanical properties of rock in both saturation and drying processes. *Rock Mech Rock Eng* 49(8):3009–3025. <https://doi.org/10.1007/s00603-016-0987-z>

Springer Nature or its licensor holds exclusive rights to this article under a publishing agreement with the author(s) or other rightsholder(s); author self-archiving of the accepted manuscript version of this article is solely governed by the terms of such publishing agreement and applicable law.